Philosophical Magazine

Publication details, including instructions for authors and subscription information:
http://www.tandfonline.com/loi/tphm20

Stacking faults and partial dislocations in graphene

M.P. Ariza [a], R. Serrano [a], J.P. Mendez [a] & M. Ortiz [b]

[a] Escuela Técnica Superior de Ingeniería, Universidad de Sevilla, Camino de los descubrimientos, s.n., 41092 Sevilla, Spain

[b] Graduate Aeronautical Laboratories, California Institute of Technology, 1200 E. California Blvd., Pasadena, CA 91125, USA

Version of record first published: 21 Feb 2012.

To cite this article: M.P. Ariza, R. Serrano, J.P. Mendez & M. Ortiz (2012): Stacking faults and partial dislocations in graphene, Philosophical Magazine, 92:16, 2004-2021

To link to this article: http://dx.doi.org/10.1080/14786435.2012.657254

Philosophical Magazine
Vol. 92, No. 16, 1 June 2012, 2004–2021

Taylor & Francis
Taylor & Francis Group

Stacking faults and partial dislocations in graphene

M.P. Ariza[a]*, R. Serrano[a], J.P. Mendez[a] and M. Ortiz[b]

[a]*Escuela Técnica Superior de Ingeniería, Universidad de Sevilla, Camino de los descubrimientos, s.n., 41092 Sevilla, Spain;* [b]*Graduate Aeronautical Laboratories, California Institute of Technology, 1200 E. California Blvd., Pasadena, CA 91125, USA*

(*Received 3 August 2011; final version received 14 December 2011*)

We investigate two mechanisms of crystallographic slip in graphene, corresponding to glide and shuffle generalized stacking faults (GSF), and compute their γ-curves using Sandia National Laboratories Large-scale Atomic/Molecular Massively Parallel Simulator (LAMMPS). We find evidence of metastable partial dislocations for the glide GSF only. The computed values of the stable and unstable stacking-fault energies are suggestive of a high stability of full dislocations against dissociation and of dislocation dipoles against annihilation.

Keywords: graphene; stacking faults; dislocations; dynamic stability

1. Introduction

Single-sheet graphene [1–3], a monolayer of sp2-bonded carbon atoms that are packed as a honeycomb crystal lattice, is actively being evaluated as a material for next-generation electronics. Thus, in addition to exceptional mechanical properties [4], pristine graphene is a ballistic conductor exhibiting remarkably high electron mobility [5,6] and thermal conductivity [7]. In addition, the potential for controlling the density of charge carriers by applying a gate voltage [2,3,6] renders graphene an attractive candidate material for electronic applications such as field-effect transistors (FETs) [1]. Graphene has been observed to be stable in free-standing form [2] and on a variety of substrates [1]. However, a number of lattice defects, including Stone–Wales (SW) defects [8], dislocation dipoles [9], and others [10], have been observed to be stable in graphene [9–12]. The stability of some of these defects has been theoretically demonstrated up to high temperatures [13]. Depending on their structure and density, these defects may have a detrimental effect on the electronic and thermal transport response of graphene, thereby limiting its potential for use in electronic applications.

Graphene defects have been analyzed by a variety of means. For instance, Jeong et al. [14] have studied the stability of dislocation dipoles with 5–7 core structure using density-functional theory. These 5–7 pairs have been observed to form complex defect structures [9]. Periodic arrangements of dislocation dipoles and quadrupoles have also been extensively considered by means of first-principles

*Corresponding author. Email: mpariza@us.es

ISSN 1478–6435 print/ISSN 1478–6443 online

http://dx.doi.org/10.1080/14786435.2012.657254
http://www.tandfonline.com

calculations [14–18]. In addition to first-principles calculations, interatomic potentials have also been widely used for modeling carbon structures in general and graphene in particular [13,19–28]. The simplest types of potential are harmonic and are defined in terms of force constants [19,25,27,28]. More general bond-order interatomic potentials include the reactive empirical bond-order (REBO) potential [24] and the reactive force field (ReaxFF) [29]. The addition of torsion, dispersion, and non-bonded repulsion interactions to the REBO potential results in a new hydrocarbon potential (AIREBO) that is suitable for studying reactivity in molecular condensed phases [26].

In this article, we investigate two mechanisms of crystallographic slip in graphene with a view to ascertaining the energetics of the resulting generalized stacking faults (GSF) and by extension, the feasibility of dislocation dissociation and the metastability of the resulting partials. The slip mechanisms are investigated within Vitek's framework of the γ-energy surface [30,31]. In order to study the stability of the dissociated dislocation cores at finite temperature, we have first computed the dislocation core structures predicted by the theory of discrete dislocations [32] and then studied their dynamic stability considering these configurations as initial conditions for a molecular dynamics calculation carried out using the Sandia National Laboratories Large-scale Atomic/Molecular Massively Parallel Simulator (LAMMPS) code [33].

2. Generalized stacking faults

The γ-surface is constructed by cutting an infinite crystal along a given crystallographic plane and then displacing the resulting half-crystals through a vector $\boldsymbol{\delta}$, or *slip displacement*, contained within the plane. An atomistic model of the crystal is then relaxed under far-field boundary conditions consistent with the slip displacement $\boldsymbol{\delta}$ and with zero normal tractions, i.e., prescribing the parallel components of the far-field displacements while simultaneously relaxing the far-field normal displacements. The resulting relaxed configurations have been termed *generalized stacking faults* (GSF) by Vitek [30]. The attendant elastic or misfit energy $\gamma(\boldsymbol{\delta})$, when plotted against the slip displacement $\boldsymbol{\delta}$, defines the so-called γ-surface of the GSF.

The two GSF geometries considered in this work, corresponding to slip across zigzag bonds and across parallel bonds, are shown in Figure 1a and b, respectively. By analogy to the diamond structure, we refer to these GSF as *glide* GSF and *shuffle* GSF, respectively (cf. e.g. [34]). For the shuffle GSF, the distance between two adjacent atomic lines on either side of the cut equals the bond length, and only one bond per atom is broken during the block-shearing process. For the glide GSF, the interplanar distance is one-half of the bond length and two bonds per atom are broken during the block-shearing process. Owing to the two-dimensionality of graphene, only one component δ of the slip displacement needs to be considered, and the γ-surfaces of the GSFs reduce to γ-*curves*. We compute the γ-curves by means of molecular dynamics calculations carried out using the Sandia National Laboratories Large-scale Atomic/Molecular Massively Parallel Simulator (LAMMPS) [33] and two different interatomic potentials: the Adaptive Intermolecular Reactive Empirical Bond-Order (AIREBO) [26] and the reactive force field (ReaxFF) [29]. Both

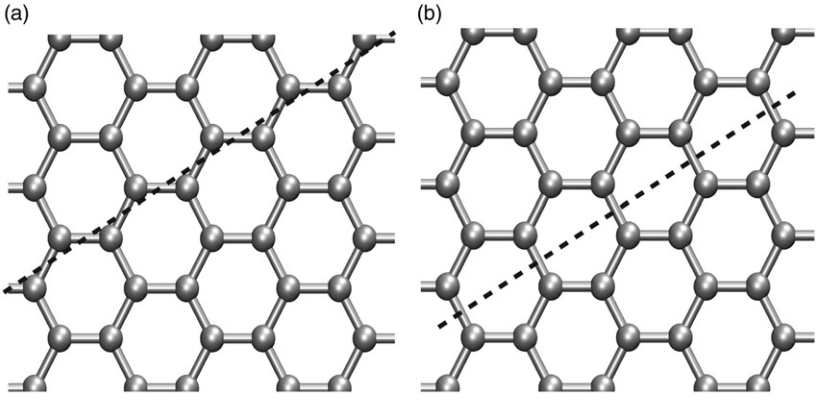

Figure 1. Generalized stacking faults considered in this study. (a) Glide GSF: slip occurs across zigzag bonds. (b) Shuffle GSF: slip occurs across parallel bonds.

potentials allow for covalent bond breaking/creation with associated changes in atomic hybridization described by means of a classical potential, thus enabling simulations of slip in single-sheet graphene. All γ-curve calculations are carried out at zero temperature [30]. By symmetry, the γ-curve is periodic of period $b = \sqrt{3}a$, where $a = 1.42$ Å is the bond length [25] and $b = 2.46$ Å is the Burgers vector size. In order to obtain the γ-curve of the glide and shuffle generalized stacking faults, the simulation cell is first cut along a zigzag direction or armchair direction, respectively (see Figure 1). Then, prescribed slip displacements in the interval $[0, b]$ are applied in increments of $b/100$ by shifting the upper part with respect to the lower part. Following Vitek [30], the far-field displacements are allowed to relax during 0.0277 ps in the direction perpendicular to the line of fault at every prescribed value of slip displacement. Periodic boundary conditions are enforced on the remaining two sides of the computational cell (Figure 2). The relaxation time after each slip is divided into 100 steps, so the time step is 0.277 fs, which satisfies the CFL condition [35]. This time step has been proposed, in order to achieve the maximal numerical stability during the simulation, by other groups working on the dynamics of graphene using MD techniques [36]. By way of comparison, we have used two different time steps, i.e., 0.1 fs and 0.277 fs, and observed that there are no differences between both simulation results.

The characteristic thermalization time required for the system to reach equilibrium may be estimated from the two-dimensional heat equation as

$$t_c = \frac{3}{2} N \frac{k_B}{K_A} \tag{1}$$

where N is the number of atoms, k_B is Boltzmann's constant, and K_A is the two-dimensional thermal conductivity of graphene. This two-dimensional thermal conductivity may in turn be estimated from the experimentally reported three-dimensional thermal conductivity K_V as $K_A = K_V h$, where h is the nominal thickness of the graphene sheet. For a periodic cell of $N = 488$ atoms, with

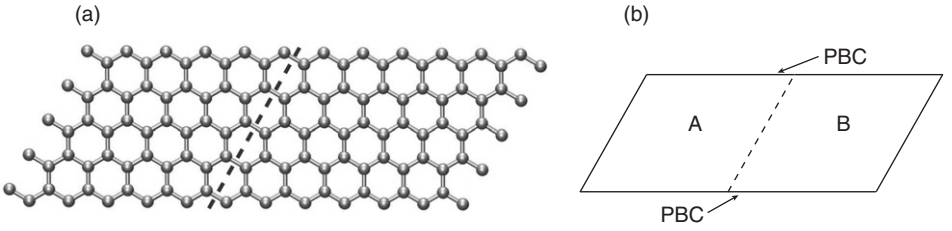

Figure 2. (a) Typical computational cell used in the analysis of stacking-fault structures in graphene. Inlaid in the figure is a schematic cut showing the plane of the stacking fault. (b) Schematic representation of Vitek's stacking fault construction. The two half graphene sheets incident on the stacking fault plane are displaced rigidly in the parallel direction. In particular, the parallel component of displacement is prescribed for all atoms. The normal component of the displacement of all atoms is unconstrained and allowed to relax as the two half-sheets slide relative to each other.

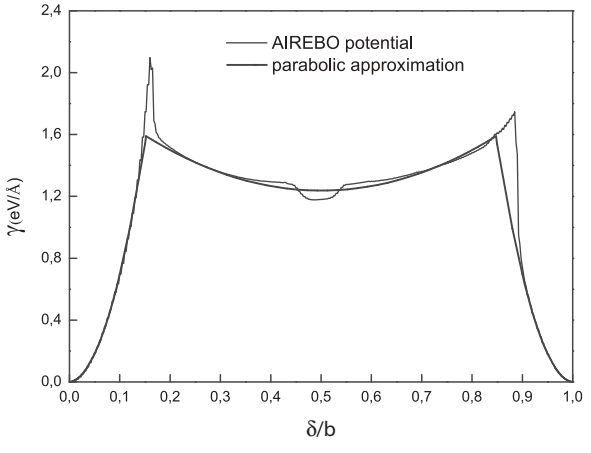

Figure 3. γ-curve of glide GSF computed from LAMMPS [33] using the AIREBO potential and its piecewise parabolic approximation.

$k_B = 1.381 \times 10^{-23}\,\mathrm{J\,K^{-1}}$, $K_V = 5 \times 10^3\,\mathrm{W\,m^{-1}\,K^{-1}}$ [37] and $h = 0.334\,\mathrm{nm}$ [38], Equation (1) gives $t_c \approx 0.0056\,\mathrm{ps}$. This estimate is smaller than the relaxation time considered after each slip.

Cells sizes ranging from 80 to 1600 atoms are used in order to assess cell-size convergence. We find that the γ-energy is ostensibly converged for a cell size of 1600 atoms.

The γ-curves for the glide GSF, Figure 1a, computed from the AIREBO and ReaxFF potentials are shown in Figures 3 and 4, respectively. Some noise notwithstanding, both potentials give strong evidence of a metastable stacking-fault configuration, or local energy minimum, at $\delta = b/2$. The computed stacking-fault energies are $\gamma_{\mathrm{sf}} = 1.18\,\mathrm{eV\,\AA^{-1}}$ for the AIREBO potential and $\gamma_{\mathrm{sf}} = 1.22\,\mathrm{eV\,\AA^{-1}}$ for the ReaxFF potential. We note that, owing to the two-dimensional geometry of graphene, the natural units for the stacking-fault energies are those of an energy per

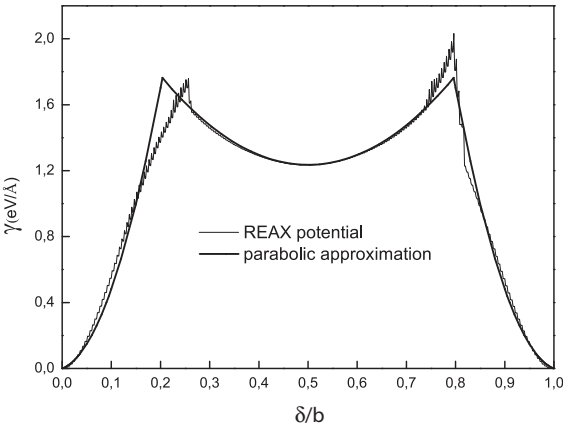

Figure 4. γ-curve of glide GSF computed from LAMMPS [33] using the ReaxFF potential and its piecewise parabolic approximation.

Table 1. Parameters of piecewise quadratic fit of the glide GSF γ-surface.

Potential	μ (eV Å^{-1})	μ_{sf} (eV Å^{-1})	γ_{sf} (eV Å^{-1})	γ_{us} (eV Å^{-1})
AIREBO	141.37	5.82	1.24	1.60
ReaxFF	89.81	12.03	1.23	1.78

unit length. The γ-curves for the glide GSF computed from the AIREBO and ReaxFF potentials are found to be well-approximated by the piecewise quadratic fit

$$\gamma(\delta) = \min\left\{\frac{\mu}{2}(\delta/b)^2, \gamma_{sf} + \frac{\mu_{sf}}{2}(\delta/b - 1/2)^2, \frac{\mu}{2}(\delta/b - 1)^2\right\}, \tag{2}$$

for δ in the interval $(0, b)$, with the function $\gamma(\delta)$ extended to the remainder of the real line by periodicity. The values of the parameters in (2) are tabulated in Table 1. The perfect lattice and the metastable stacking-fault configurations are separated by unstable stacking-fault configurations at slip displacements $\delta = 0.15b$ for the AIREBO potential and $\delta = 0.20b$ for the ReaxFF potential (parabolic approximation). The corresponding unstable stacking-fault energies, i.e., the energy barrier separating the perfect lattice and the stable stacking-fault configuration, are computed to be $\gamma_{us} = 1.60\,\text{eV Å}^{-1}$ for the AIREBO potential and $\gamma_{us} = 1.78\,\text{eV Å}^{-1}$ for the ReaxFF potential.

The piecewise quadratic fits of the AIREBO and ReaxFF γ-curves for the glide GSF are compared in Figure 5. Remarkably, the values of the stacking-fault energy γ_{sf} predicted by the AIREBO and ReaxFF potentials are nearly identical. By contrast, the AIREBO potential predicts a somewhat lower unstable stacking-fault energy than that predicted by the ReaxFF. Closeup views of the relaxed atomic structure of the unstable and stable stacking faults are also inset in Figure 5. In order

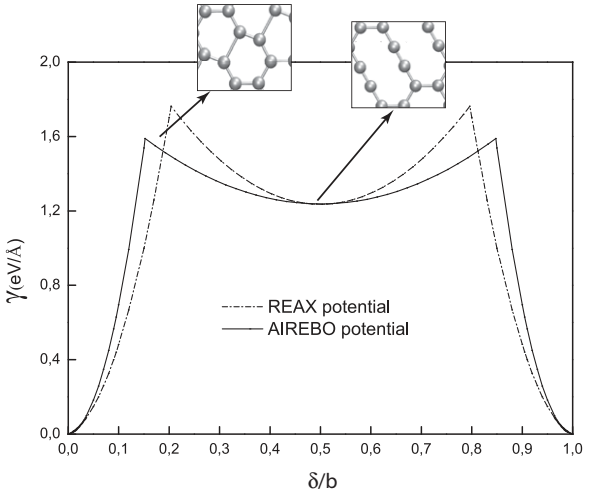

Figure 5. Piecewise parabolic approximations of the γ-curves of a glide GSF computed from the AIREBO and ReaxFF potentials. Details of the stable and unstable stacking-fault atomic configurations at 0 K are also inset in the figure.

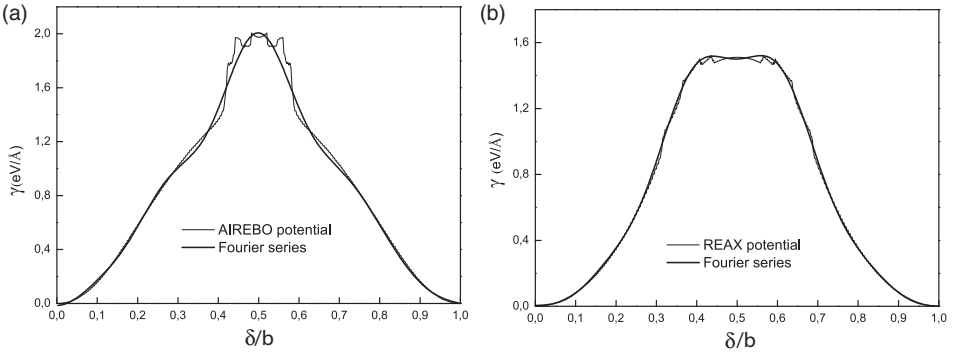

Figure 6. γ curve of shuffle dislocation computed from LAMMPS [33] using (a) the AIREBO potential and its Fourier series approximation and (b) the ReaxFF potential and its Fourier series approximation.

to verify the stability of the latter atomic structure configuration, we have allow the system to relax over a time of 1000 ps, which, according to the previous estimate (1), amply suffices for the system to reach thermal equilibrium. As may be seen from the figure, the unstable stacking-fault configuration consists of a distorted hexagonal lattice, whereas the stable stacking-fault configuration consists of an array of decarings.

Next we turn to the shuffle GSF, Figure 1b. The γ-curves for the shuffle GSF computed from the AIREBO and ReaxFF potentials are shown in Figure 6a and b, respectively. As is evident from the figure, the γ-curve predicted by the ReaxFF

Table 2. Parameters of an 11-term cosine Fourier series fit of the shuffle GSF γ-surface.

Potential	c_1	c_3	c_5	c_7	c_9	c_{11}
AIREBO	1.139	−0.826	−0.413	0.128	0.041	−0.061
ReaxFF	0.968	−0.737	−0.413	0.150	0.015	0.026
	c_{13}	c_{15}	c_{17}	c_{19}	c_{21}	γ_{us} (eV Å^{-1})
AIREBO	−0.080	0.064	0.039	−0.026	−0.019	1.97
ReaxFF	0.033	−0.035	−0.033	0.023	0.011	1.51

potential is somewhat softer than that predicted by the AIREBO potential. Contrary to the case of the glide GSF and differences in fine structure notwithstanding, both potentials rule out the existence of a stable stacking-fault configuration for the shuffle GSF. Instead, both the AIREBO and ReaxFF potentials predict unstable stacking-fault configurations at $\delta = b/2$ of unstable stacking-fault energies $\gamma_{us} = 1.97\,\text{eV Å}^{-1}$ and $\gamma_{us} = 1.51\,\text{eV Å}^{-1}$, respectively. Owing to the b-periodicity and evenness of the γ-curves, a cosine Fourier series representation of the form

$$\gamma(\delta) = \gamma_{us} \sum_{n=1}^{N} c_n \cos \frac{n\pi\delta}{2b} \tag{3}$$

suggests itself as an analytical approximation to the computed curves. The coefficients of a 11-term expansion are collected in Table 2.

The Fourier series fits of the AIREBO and ReaxFF γ-curves for the shuffle GSF are shown in Figure 6a and b. As already noted, the ReaxFF-potential γ-curve undershoots the AIREBO-potential γ-curve, and both curves differ in fine detail, the AIREBO-potential γ-curve exhibiting a wavier profile. As for the glide GSF, a closeup view of the atomic structure of the unstable stacking-fault has been inset in Figure 7. Similarly to the unstable glide stacking-fault configuration, a distorted hexagonal lattice has been observed.

3. The lattice complex of graphene and its harmonic approximation

In this section we summarize the specialization to graphene [13,28] of the general theory of discrete dislocation in crystal lattice developed by the authors [32]. The primary objective of this section is to present a general expression for the stored energy of the graphene crystal in terms of eigendeformations. Following [32], we regard the graphene lattice as a *cell-complex* $\mathcal{C}$, i.e., as a collection of cells of different dimensions equipped with discrete differential operators and a discrete integral. In particular, the graphene complex is two-dimensional and consists of: atoms, or 0-cells; atomics bonds, or 1-cells; and hexagonal cells, or 2-cells, Figure 8. For ease of indexing, we denote by $E_p(\mathcal{C})$ the collection of all cells of dimension $p = 0, 1, 2$ in the graphene cell complex $\mathcal{C}$. These cells supply the support for defining functions, or *forms*, of different dimensions. Thus, of dimension p assign vectors to each cell of dimension p of the lattice. In particular, we refer a function defined over the atoms as a 0-form, a function defined over the atomic bonds as a 1-form and a function

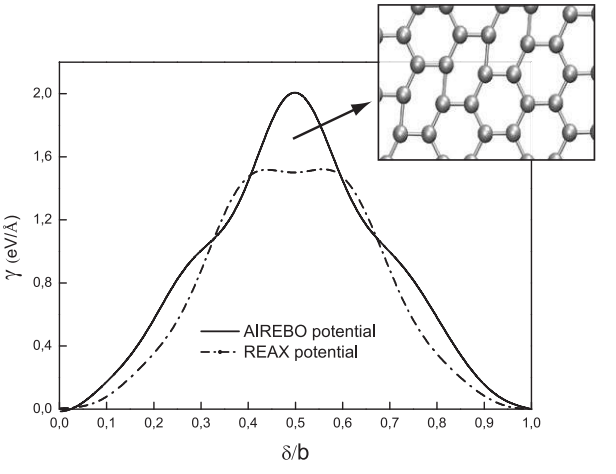

Figure 7. Fourier series approximations of the γ-curves of a shuffle dislocation computed from the AIREBO and ReaxFF potentials. Details of atomic configurations at 0 K are also inset in the figure.

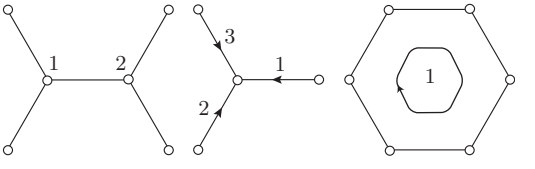

Figure 8. The oriented 0, 1 and 2-cells of graphene grouped by type.

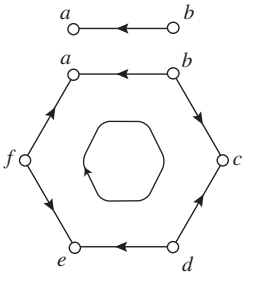

Figure 9. Diagram for the definition of the discrete differential operators of graphene.

defined over the hexagonal cells as a 2-form. As we shall see, forms provide the vehicle for describing the behavior of the graphene lattice, including its displacements, eigendeformations and dislocation densities.

In order to define the *discrete differential operators* of the lattice, we begin by orienting all cells, Figure 8. Suppose that ω is a 0-form defined over the atoms and let e_{ab} be an atomic bond defined by atoms a and b, cf. Figure 9. Suppose,

in addition, that e_{ab} is oriented from a to b. Then, the differential $d\omega(e_{ab})$ of ω at e_{ab} is

$$\mathrm{d}\omega(e_{ab}) = \omega(e_b) - \omega(e_a). \tag{4}$$

Suppose now that ω is a 1-form defined over the atomic bonds and let e_{abcdef} be a hexagonal cell bounded by the atomic bonds e_{ab}, e_{bc}, e_{cd}, e_{de}, e_{ef} and e_{abcdef}, cf. Figure 9. Then, the differential $d\omega(e_{ab})$ of ω at e_{abcdef} is

$$\mathrm{d}\omega(e_{abcdef}) = \omega(e_{ab}) + \omega(e_{bc}) + \omega(e_{cd}) + \omega(e_{de}) + \omega(e_{ef}) + \omega(e_{fa}). \tag{5}$$

Finally, ω is a 2-form defined over the hexagonal cells. Then, its differential is the vector

$$\mathrm{d}\omega = \sum_{e_2 \in E_2(\mathcal{C})} \omega(e_2). \tag{6}$$

Thus, the differential operator maps: 0-forms, defined over the atoms, to 1-forms, defined over the atomic bonds; 1-forms, defined over the atomic bonds, to 2-forms, defined over the hexagonal cells; and 2-forms, defined over the hexagonal cells, to vectors. The discrete differential operators thus defined may be regarded as the discrete counterparts of the familiar grad, curl and div of vector calculus. In particular, the differential of 0-forms is the discrete counterpart of the grad operator; the differential of 1-forms is the discrete counterpart of the curl operator; and the differential of 2-forms is the discrete counterpart of the div operator from vector calculus. It is readily verified from the definition of the discrete differential operators that

$$d^2 = 0, \tag{7}$$

which is the discrete counterpart of the identities $\mathrm{curl} \circ \mathrm{grad} = 0$ and $\mathrm{div} \circ \mathrm{curl} = 0$.

By grouping cells of the same type (Figure 8), it may be observed that they are translations of each other and have the same complement of neighbors, or *environment*. According to this definition, graphene has two types of atoms, three types of atomic bonds and one type of hexagonal cell. The fundamental property of cells of the same type is that they are arranged as *simple Bravais lattices*, Figure 10. Thus, the atoms of graphene define two simple Bravais lattices, the atomic bonds define three simple Bravais lattices, and the hexagonal cells define one simple Bravais lattice. Consequently, the Discrete Fourier Transform (DFT) provides a natural tool for the analysis of discrete forms, cf., e.g., [32,39]. Thus, the DFT of a p-form ω is

$$\hat{\omega}(\theta, \alpha) = \sum_{l \in \mathbb{Z}^2} \omega(l, \alpha) \mathrm{e}^{-i\theta \cdot l} \tag{8}$$

where $l \in \mathbb{Z}^2$ and θ range over $[-\pi, \pi]^2$. Similarly, the corresponding DFT representation of the differential $d\omega$ is

$$\widehat{d\omega}(\theta, \alpha) = \sum_{\beta=1}^{N_p} Q\begin{pmatrix} \theta \\ \alpha \quad \beta \end{pmatrix} \hat{\omega}(\theta, \beta) \tag{9}$$

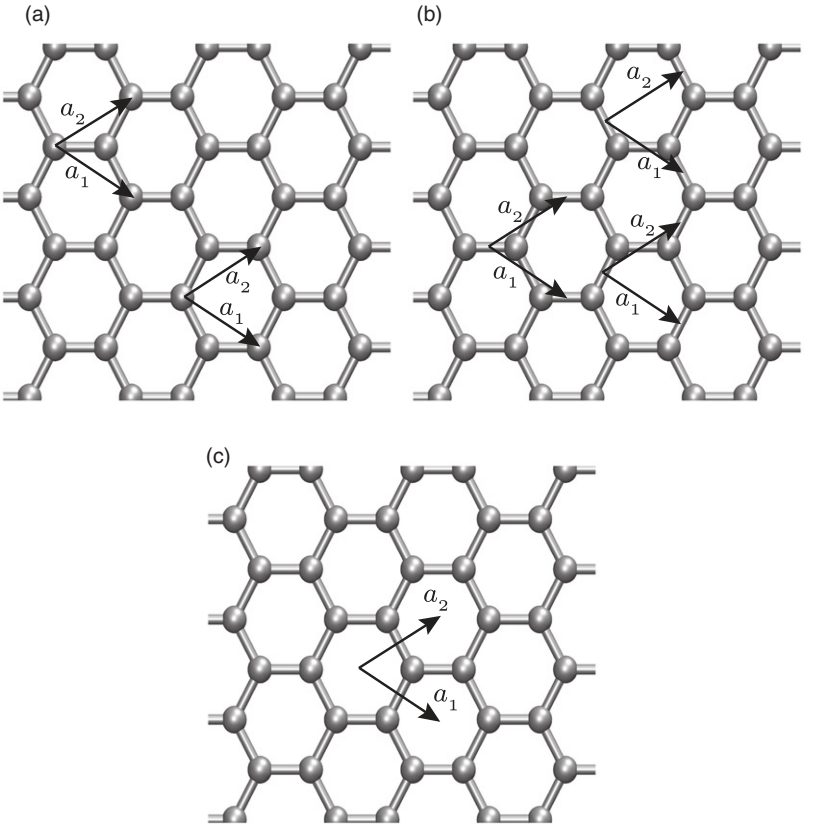

Figure 10. The simple Bravais lattices defined by the atoms, atomic bonds and hexagonal cells of graphene.

where the coefficients $Q\left(\begin{smallmatrix}\theta\\ \alpha\ \beta\end{smallmatrix}\right)$ represent the differential operator defined over the lattice.

It is possible to fashion a theory of discrete dislocations in crystals from the classical *theory of eigendeformations*, cf., e.g., [40]. Based on the fundamental property of crystals, that certain uniform deformations leave the crystal lattice unchanged and, hence, should cost no energy, the energy of the crystal may be written as

$$E(u,\beta) = \frac{1}{2}\sum_{e_1\in E_1(\mathcal{C})}\sum_{e_1'\in E_1(\mathcal{C})}\langle B(e_1,e_1')(du(e_1)-\beta(e_1)),(du(e_1')-\beta(e_1'))\rangle$$
$$\equiv \frac{1}{2}\langle B(du-\beta),(du-\beta)\rangle \tag{10}$$

where the sums take place over the atomic bonds of the crystal lattice, and $u(e_0)$ is the atomic displacement of atom e_0, d$u(e_1)$ is the deformation of atomic bond e_1, $\beta(e_1)$ is the eigendeformation at bond e_1, and $B(e_1,e_1')$ are bond-wise force constants giving the interaction energy resulting from a unit differential displacement at bond e_1' and a

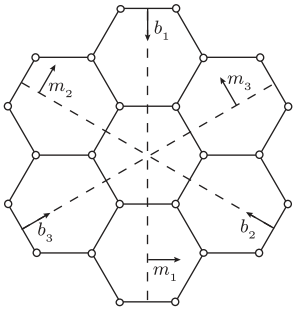

Figure 11. Fundamental lattice-preserving shear deformations of graphene considered in this work.

unit differential displacement at bond e_1. Explicit expressions of the force-constant values from the AIREBO potential (Adaptive Intermolecular Reactive Empirical Bond-Order) [26] and from the potential of Aizawa et al. [25] have been previously obtained [28,41].

In (10), the local values $\beta(e_1)$ of the eigendeformation field are constrained to defining lattice-invariant deformations. By this restriction and the form of the energy (10), uniform lattice-invariant deformations du cost no energy, as desired. We note that, owing to the discrete nature of the set of lattice-invariant deformations, the energy (10) is strongly nonlinear. In particular, the reduced energy

$$E(u) = \inf_{\beta} E(u, \beta) \tag{11}$$

is piecewise quadratic with zero-energy wells at all uniform lattice-invariant deformations.

The entire class of lattice-invariant deformations is characterized by a classical theorem of Ericksen [42] as the set of unimodular affine mappings with integer lattice coordinates. The ones considered in this work are shown in Figure 11. The stored energy of a crystal may be obtained by minimizing (10) with respect to u

$$\inf_{u} E(u, \beta) = E(\beta) \tag{12}$$

which is strongly nonlinear by the constraint that the local Burgers vectors must be integer linear combinations of the basic Burgers vectors b_i in Figure 11 (see [13,28]).

4. Dynamic stability at finite temperature

In this section we study the stability of dissociated dislocation cores and the metastability of the resulting partials. Recent publications have extensively discussed the formation of structural defects in graphene, in particular, the ability of graphene to reconstruct its lattice around intrinsic defects [43] or the existence of arrays of edge dislocations associated to graphene grain boundaries [44]. We have first studied the structural transformation and stability of the stable stacking-fault configuration at finite temperature by considering this configuration as initial conditions for a

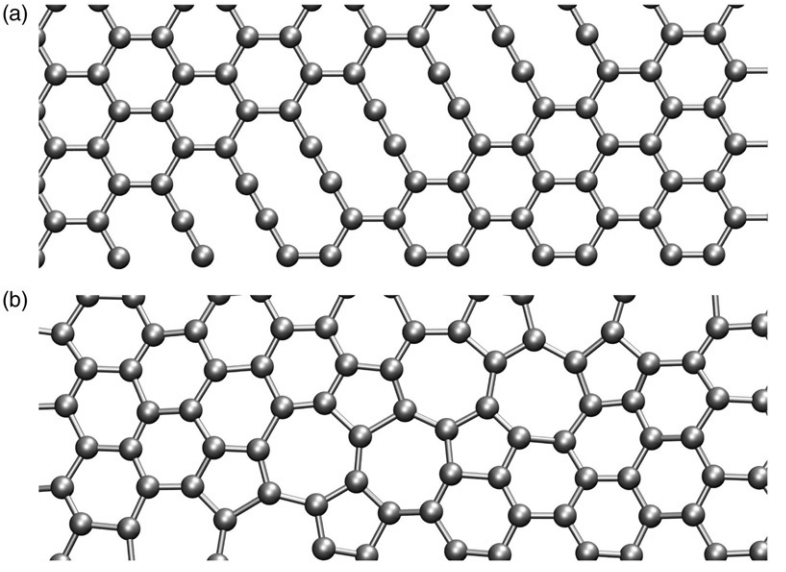

Figure 12. Stable glide stacking-fault atomic configuration at two different temperatures after relaxation: (a) up to 300 K; (b) up to 1500 K.

molecular dynamics calculation based on the AIREBO potential [26] and carried out using LAMMPS. The observed initial array of decarings (Figure 12a) remains stable up to temperatures of 1500 K, whereas it transforms into two parallel chains of pentagon-heptagon pairs (5|7) at higher temperatures up to 2700 K (Figure 12b). Regular arrays of (5|7) pairs have been observed at the edges of misoriented graphene grain boundaries, in particular between armchair and zigzag edge orientations [43,44].

The γ-surfaces of a crystal shed useful light on the structure and stability of extended defects such as dislocation dipoles and dissociated cores. Consider, for instance, the stability of a glide dislocation dipole against annealing. To this end, we consider two competing configurations of the dipole, one in which two perfect configurations are separated by a distance d and another, the transition state, in which the perfect dislocations are replaced by two adjacent $b/2$ partials each. The dipole is unstable if the elastic energy released by the transition exceeds the energy barrier $\gamma_{\mathrm{us}}b$, leading to a stability condition

$$\frac{Kb^2}{4\pi d} \leq \gamma_{\mathrm{us}}. \tag{13}$$

Equivalently, the spontaneous pair-annihilation distance follows as

$$d_c = \frac{Kb^2}{4\pi\gamma_{\mathrm{us}}}. \tag{14}$$

Inserting into (14) the prelogarithmic factor $K = 15.486\,\mathrm{eV\,\AA^{-2}}$ computed by Ariza and Ortiz [28] using the potential of Aizawa et al. [25], as well as the value of the

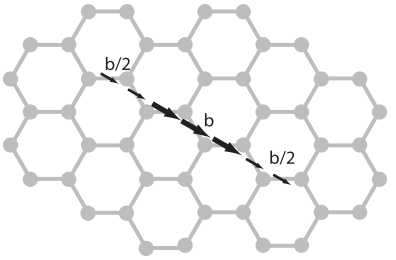

Figure 13. Detail of the distribution of eigendeformations $\beta_i(e_1)$, consisting of one Burgers vector over a zigzag chain of n one-cells and half Burgers vector over two zigzag chains of m one-cells on the left and right of the first one.

unstable stacking-fault energy $\gamma_{\text{us}} = 1.60\,\text{eV}\,\text{Å}^{-1}$ computed from the AIREBO potential, we obtain $d_c \simeq 1.9b$. A somewhat smaller critical distance is computed from the ReaxFF potential. These simple estimates suggest that dislocation dipoles are stable in graphene down to exceedingly small separations of the order of a few lattice spacings. This finding is consistent with the finite-temperature LAMMPS calculations of Ariza et al. [13], who showed that dislocation quadrupoles are compact as $8b$ in size are indeed dynamically stable up to temperatures of 2500 K.

Consider now the dissociation of glide dislocations into $b/2$-partials separated by stacking-fault ribbons, resulting in *extended cores*. In this case, balancing the repulsive elastic force and the configurational force corresponding to the size of a stacking-fault ribbon gives the force-balance equation (e.g., [45])

$$\frac{K(b/2)^2}{4\pi d} = \gamma_{\text{sf}}, \tag{15}$$

whence the equilibrium separation between partials follows as

$$d_{\text{eq}} = \frac{Kb^2}{16\pi\gamma_{\text{sf}}}. \tag{16}$$

Inserting again the prelogarithmic factor $K = 15.486\,\text{eV}\,\text{Å}^{-2}$ computed by Ariza and Ortiz [28] using the potential of Aizawa et al. [25], as well as the value of the stacking-fault energy $\gamma_{\text{sf}} = 1.24\,\text{eV}\,\text{Å}^{-1}$ computed from the AIREBO potential, we obtain $d_{\text{eq}} \simeq 0.61b$. It follows from this estimate that dissociation into partials is unlikely in graphene. Again, this conclusion is born out by direct molecular dynamics calculations (cf., e.g., [13]) which are suggestive of the stability against dissociation of graphene dislocations up to temperatures of 2500 K.

Next, using the theory of discrete dislocations outlined in Section 3, we proceed to further investigate the stability of dissociated cores in graphene. In particular, we compute the displacement fields and the energies of periodic distributions of dissociated dipoles in the configuration shown in Figure 13. The corresponding eigendeformation field consists of one Burgers vector over a zigzag chain of n one-cells and half Burgers vector over two zigzag chains of m one-cells at the left and right ends ($m-n-m$). We begin by considering periodic distributions of type $m-n-m$ with increasing values of n and $m=2$. The initial discrete dislocation

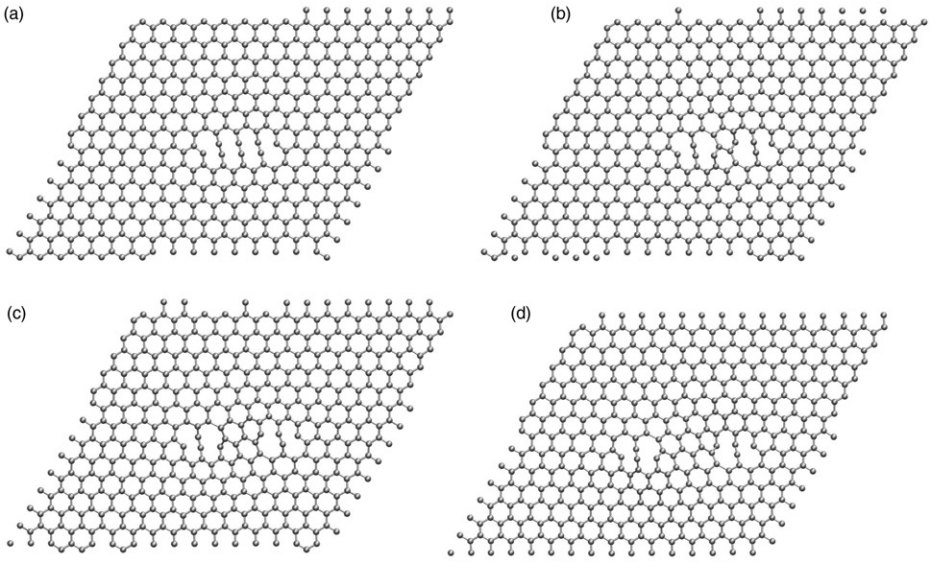

Figure 14. Deformed configurations of periodic arrangement of discrete dislocations for a 448-atom unit cell containing 2-*n*-2 configuration at finite temperature: (a) $n=3$; (b) $n=5$; (c) $n=7$; (d) $n=9$.

configuration is first allowed to relax at 0 K in order for the system to reach thermal equilibrium. Then we proceed to increase the temperature while simultaneously allowing time for relaxation. The dynamic stability at finite temperature of a sequence of configurations with values of n ranging from 3 to 9 is observed to be roughly independent of the value of n (Figure 14). In particular, the atomic configuration corresponding to dislocation partials (two decarings) remains stable up to 300 K over long periods of time for all values of n considered. At higher temperatures, between 300 K and 400 K, the partials recombine. For the 2-3-2 configuration, which contains two consecutive pairs of two decarings, the partials do not transform into 5–7 pairs at any finite temperature. However, the defective system evolves toward a defect free lattice at a temperature range between 350 to 400 K (Figure 15). The transformations for the rest of configurations give rise to the pattern observed when the defect contained in the computational cell is a perfect dipole of length n atomic bonds (Figure 16). All LAMMPS calculations are carried out at fixed constant temperature using the Nose–Hoover thermostat. The tabulated energies are time-averaged total energies (potential plus kinetic) of the defects, i.e., the total energy of the lattice with defects minus the total energy of the lattice without defects.

Table 3 compares the defect energies of two different initial configurations of defects at different temperatures. The first configuration corresponds to a $m-n-m$ defect (Figure 13), whereas the second corresponds to a dipole of length n. In both these cases, defects are embedded in periodic cells of 448 atoms. The results are suggestive of a high stability of full dislocations against dissociation and of dislocation dipoles against annihilation.

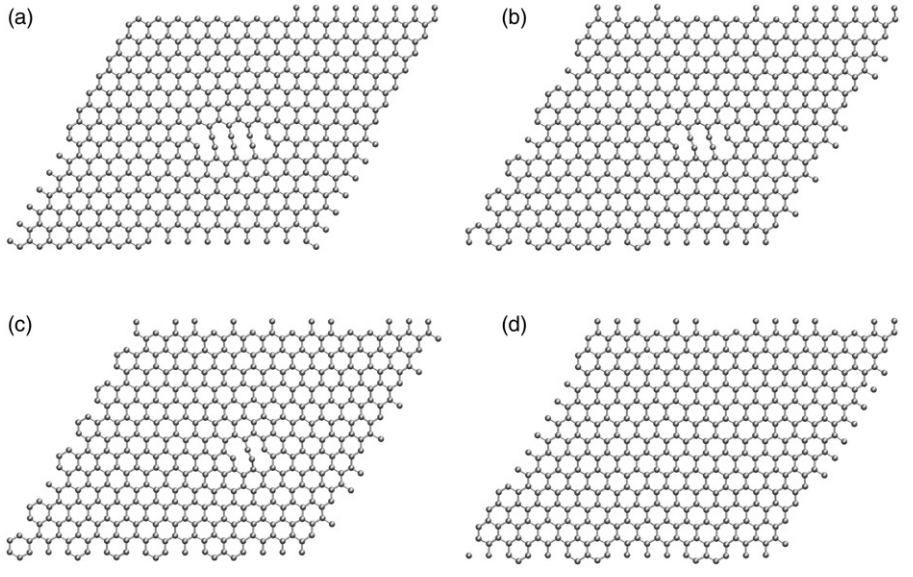

Figure 15. Evolution of the 2-3-2 defective configuration toward a defect-free lattice at a temperature range between 350 to 400 K.

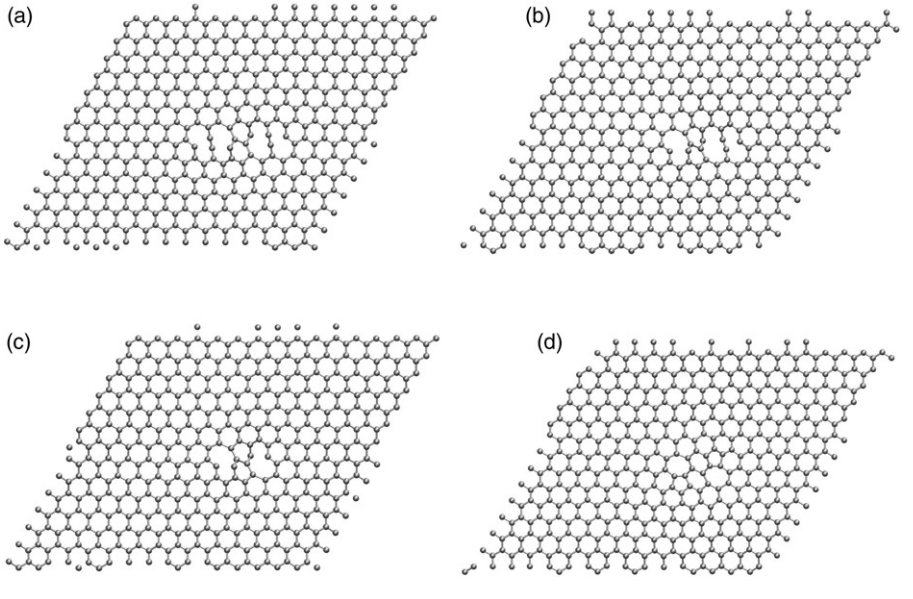

Figure 16. Deformed configurations of periodic arrangement of discrete dislocations for a 448-atom unit cell containing 2-5-2 configuration at finite temperature: (a) up to 300 K; (b) 350 K; (c) 400 K. (d) 500 K.

Table 3. Defect energy (eV) values after relaxation of 2-*n*-2 configuration and a dipole of length *n* embedded in a 448-atom unit periodic cell at different temperatures.

	0 K	500 K
2-5-2	22.70	10.47
dipole $L = 5$	12.73	10.44
2-7-2	26.06	13.81
dipole $L = 7$	13.49	13.80

The out-of-plane displacements of the atoms bear special remark. In all cases, be it the discrete dislocation calculations or the full LAMMPS molecular dynamics calculations, the displacements of the atoms out of the plane of the graphene sheet are unconstrained. However, in the 0 K discrete dislocation calculations the out-of-plane displacements vanish, an indication that the planar geometry of the sheet is locally stable at 0 K, even in the presence of defects, though not necessarily globally stable when the full interatomic potential is taken into account. By contrast, in the LAMMPS molecular dynamics calculations at finite temperature, the dislocation cores deviate from planarity, and the out-of-plane displacements of the atoms are of the same order as the in-plane ones.

5. Conclusions

In this paper we have studied two mechanisms of crystallographic slip in graphene, corresponding to glide and shuffle generalized stacking faults (GSF). These calculations have been performed using the Sandia National Laboratories Large-scale Atomic/Molecular Massively Parallel Simulator (LAMMPS) and two different interatomic reactive potentials: the Adaptive Intermolecular Reactive Empirical Bond-Order (AIREBO) and the reactive force field (ReaxFF). We report the existence of metastable partial dislocations for the glide GSF, whereas no stable stacking-fault configuration is observed for the shuffle GSF. Furthermore, we have investigated the stability of dissociated dislocation cores at finite temperature. In particular, after computing the atomic structures predicted by the theory of discrete dislocations, we have studied their dynamic stability considering these atomic configurations as initial conditions for a molecular dynamics calculation carried out using LAMMPS. Our simulations indicate that annihilation of dislocation dipoles and dissociation of perfect dislocations into partials in graphene are unlikely.

Acknowledgments

We gratefully acknowledge the support of the Ministerio de Ciencia e Innovación of Spain (DPI2009-14305-C02-01) and the support of the Consejería de Innovación of Junta de Andalucía (P09-TEP-4493). Support for this study was also provided by the Department of Energy National Nuclear Security Administration under Award Number DE-FC52-08NA28613 through Caltech's ASC/PSAAP Center for the Predictive Modeling and Simulation of High Energy Density Dynamic Response of Materials.

References

[1] K.S. Novoselov, A.K. Geim, S.V. Morozov, D. Jiang, Y. Zhang, S.V. Dubonos, I.V. Grigorieva and A. Firso, Science 306 (2004) p.666.
[2] J.C. Meyer, A.K. Geim, M.I. Katsnelson, K.S. Novoselov, T.J. Booth and S. Roth, Nature 446 (2007) p.60.
[3] A.K. Geim and K.S. Novoselov, Nature Mater. 6 (2007) p.183.
[4] I.W. Frank, D.M. Tanenbaum, A.M. Van der Zande and P.L. McEuen, J. Vacuum Sci. Technol. B 25 (2007) p.2558.
[5] K. Bolotin, K. Sikes, Z. Jiang, M. Klima, G. Fudenberg, J. Hone, P. Kim and H. Stormer, Solid State Commun. 146 (2008) p.351.
[6] A.H. Castro Neto, F. Guinea, N.M.R. Peres, K.S. Novoselov and A.K. Geim, Rev. Mod. Phys. 81 (2009) p.109.
[7] A. Balandin, S. Ghosh, W. Bao, I. Calizo, D. Teweldebrhan, F. Miao and C. Lau, Nano Lett. 8 (2008) p.902.
[8] A. Stone and D. Wales, Chem. Phys. Lett. 128 (1986) p.501.
[9] A. Hashimoto, K. Suenaga, A. Gloter, K. Urita and S. Iijima, Nature 430 (2004) p.870.
[10] J.C. Meyer, C. Kisielowski, R. Erni, M.D. Rossell, M.F. Crommie and A. Zettl, Nano Lett. 8 (2008) p.3582.
[11] G.M. Rutter, J.N. Crain, N.P. Guisinger, T. Li, P.N. First and J.A. Stroscio, Science 317 (2007) p.219.
[12] R.H. Telling and M.I. Heggie, Phil. Mag. 87 (2007) p.4797.
[13] M.P. Ariza, M. Ortiz and R. Serrano, Internat. J. Fracture 166 (2010) p.215.
[14] B.W. Jeong, J. Ihm and G.D. Lee, Phys. Rev. B 78 (2008), Article No. 165403.
[15] L. Li, S. Reich and J. Robertson, Phy. Rev. B 72 (2005), Article No. 184109.
[16] E. Kaxiras and K.C. Pandey, Phys. Rev. Lett. 61 (1988) p.2693.
[17] C.H. Xu, C.L. Fu and D. Pedraza, Phy. Rev. B 48 (1993) p.13273.
[18] J.H. Los, L.M. Ghiringhelli, E.J. Meijer and A. Fasolino, Phys. Rev. B 72 (2005), Article No. 214102.
[19] L. Wirtz and A. Rubio, Solid State Commun. 131 (2004) p.141.
[20] L.A. Falkovsky, Phys. Lett. A 372 (2008) p.5189.
[21] N. Mounet and N. Marzari, Phys. Rev. B 71 (2005), Article No. 205214.
[22] A. Grüneis, R. Saito, T. Kimura, L.G. Cançado, M.A. Pimenta, A. Jorio, A.G. Souza Filho, G. Dresselhaus and M.S. Dresselhaus, Phys. Rev. B 65 (2002), Article No. 155405.
[23] J. Tersoff, Phys. Rev. B 37 (1988) p.6991.
[24] D.W. Brenner, Phys. Rev. B 42 (1990) p.9458.
[25] T. Aizawa, R. Souda, S. Otani, Y. Ishizawa and C. Oshima, Phys. Rev. B 42 (1990) p.11469.
[26] S.J. Stuart, A.B. Tutein and J.A. Harrison, J. Chem. Phys. 112 (2000) p.6472.
[27] V.K. Tewary and B. Yang, Phys. Rev. B 79 (2009), Article No. 075442.
[28] M.P. Ariza and M. Ortiz, J. Mech. Phys. Solids 58 (2010) p.710.
[29] A.C.T. Duinvan, S. Dasgupta, F. Lorant and W.A. Goddard III, J. Phys. Chem. A 105 (2001) p.9396.
[30] V. Vitek, Phil. Mag. A 18 (1968) p.773.
[31] J.W. Christian and V. Vitek, Rep. Prog. Phys. 33 (1970) p.307.
[32] M.P. Ariza and M. Ortiz, Arch. Rat. Mech. Anal. 178 (2005) p.149.
[33] S.J. Plimpton, J. Comput. Phys. 117 (1995), http://lammps.sandia.gov, p.1.
[34] Y.M. Juan and E. Kaxiras, Phil. Mag. A 74 (1996) p.1367.
[35] R. Courant, K. Friedrichs and H. Lewy, Math. Ann. 100 (1928) p.32.
[36] M.S. Jang, H. Kim, H.A. Atwater and W.A. Goddard III, Appl. Phys. Lett. 97 (2010), Article No. 043504.

[37] M.S. Fuhrer, C.N. Lau and A.H. MacDonald, MRS Bull. 35 (2010) p.289.
[38] Y. Baskin and L. Meyer, Phys. Rev. 100 (1955) p.544.
[39] I. Babuska, E. Vitasek and F. Kroupa, Czech. J. Phys. B 10 (1960) p.419.
[40] T. Mura, *Micromechanics of defects in solids*, Kluwer Academic Publishers, Boston, 1987.
[41] M.P. Ariza, C. Ventura and M. Ortiz, Revista Internacional Metodos Numericos para Calculo y Diseño en Ingenieria 27 (2011) p.105.
[42] J.L. Ericksen, Arch. Rat. Mech. Anal. 72 (1979) p.1.
[43] F. Banhart, J. Kotakoski and A. Krasheninnikov, ACS Nano 5 (2011) p.26.
[44] T.H. Liu, G. Gajewski, C.W. Pao and C.C. Chang, Carbon 49 (2011) p.2306.
[45] J.P. Hirth and J. Lothe, *Theory of Dislocations*, McGraw-Hill, New York, 1968.